Frontiers in Heat and Mass Transfer (FHMT), 11, 33 (2018)
DOI: 10.5098/hmt.11.33

Global Digital Central
ISSN: 2151-8629

Frontiers in Heat and Mass Transfer

Available at www.ThermalFluidsCentral.org

DEVELOPMENT OF NEW CORRELATIONS FOR NUSSELT NUMBER AND FRICTION FACTOR OF TiO_2/WATER BASED NANOFLUID FLOW IN V-PATTERN PROTRUSION RIBBED SQUARE CHANNEL

Yashwant Singh[a], Rajesh Maithani[b], Sunil Kumar[a], Ehsan Gholamalizadeh[c], Anil Kumar[a,d*]

[a]*School of Mechanical and Civil Engineering, Shoolini University, Solan, HP, 173212, India*
[b]*Department of Mechanical Engineering, DIT University, Dehradun, Uttarakhand, 248009, India*
[c]*Department of Mechanical Engineering, Sejong University, Seoul, 100083, Republic of Korea*
[d]*Himalayan Centre of Excellence in Nanotechnology, Shoolini University, Solan, 173212, India*

ABSTRACT

Nanofluids play important roles in the heat transfer and flow characteristics in ribbed square channels. Systematic experiments are conducted to measure heat transfer enhancement and $TiO_2 - H_2O$ based nanofluid flow characteristics on a protruded with combined V-type ribbed square channel. Reynolds number studied in the channel range from 4000-18000. Investigational parameters of square channel contain, volume fraction range of 1.0-4.0%, particle diameter range of 30nm-45nm, relative protruded rib height range of 0.10-0.25, ratio of protruded height to print diameter range of 0.8-2.0, relative protruded rib pitch ratio range of 2.0-3.5 and angle of attack of 30^0-75^0 respectively. Results indicates that the thermal performance of the protruded combined V-type ribbed square channel falls with increasing Reynolds number. The highest value of thermal hydraulic performance parameter is found to be 3.21for the range of parameters investigated. Correlations predicting Nusselt number and friction factor as a function of volume fraction, particle diameter range, relative protruded rib height, ratio of protruded height to print diameter, relative protruded rib pitch ratio, angle of attack and flow parameter. The correlations for Nusselt number and friction factor have also been developed on the basis of experimental data with considerable good accuracy.

Keywords: *Nano powder, energy, flow duct, friction factor, single phase heat transfer.*

1. INTRODUCTION

Nanofluids are attracting number of investigators for their better thermo-physical properties with low penalty flow friction. Nanofluids, the new generation heat transfer medium, are studied in many heat transfer processes due to its high heat transfer enhancement performance and stability. The successful employment of nanofluids makes the heat transfer equipment more portable and smaller, so the process of miniaturization of heat transfer devices is accelerated (Ganvir et al., 2017). In recent years, many studies have yet been conducted on the heat transfer performance of nanofluids. The subject of giving more powerful and reliable thermal system in reducing the size, weight, cost, and saving of energy has gotten significant consideration. Therefore, energy cost and ecological concerns are going ahead to urge endeavors to imagine better execution over the current outlines. Keeping in mind the end goal to accomplish these requests, numerous generation strategies have been investigated over the years (Fang et al., 2016; Sarkar, 2011). The repeated rib surfaces are known for their effective enhancement of heat transfer, which is widely demanded in many scientific and industrial applications (Kumar et al., 2017a; Kumar et al., 2017b). Utilizing ribs on the internal surface of heat exchangers has been one of the normal in dynamic strategies to breakdown the laminar sub-layer and produce local wall turbulence because of stream partition and reattachment between consecutive corrugations, which directs the thermal resistance and expressively expands heat exchange (Duangthongsuk and Wongwises, 2009). Pourdel et al. (2018) numerically analyzed the fluid flow and heat transfer of a flat tube under the constant heat flux using finite volume method and SIMPLE algorithm. Their results showed that by increasing Reynolds number, the convection heat transfer (Nusselt number) and the friction factor rise. Also, by decreasing the dimensionless pitch and increasing the dimensionless depth of dimple, Nusselt number and friction factor increase.

Forced convection augmentation is obtained by means of several techniques in thermal devices development and it allows to realize size reduction and efficiency factor improvement. The grooved entry, because of its adequacy in heat exchange, is a decent hope for engineering applications for example cross-stream heat exchanger, gas turbine airfoil cooling plan, solar air heater blade cooling system and gas cooled atomic reactor (Tiwari et al., 2013). A lot of information are available is forced convection flow over a ribbed surface channels and tubes. Several scientists have investigated characteristics of nanofluids such as (Navaei et al., 2015) investigated the consequence of three different rib–groove shapes (rectangular, semi-circular and trapezoidal). Four different types of nanoparticles, Al_2O_3, CuO, SiO_2 *and* ZnO with different volume fractions in the range of 1% to 4% and different nanoparticle diameters in the range of 20 nm to 60 nm. Simulation results reveal that the semi-circular rib–groove has the highest Nusselt number. The nanofluid containing SiO_2 has the highest Nusselt number compared with other types. The Nusselt number rises as volume fraction increases, and it declines as the nanoparticle diameter increases. Ahn et al. (2010) examined the augmentation of nucleate boiling critical heat flux (CHF) by means of nanofluids stream in a pool boiling are well-known. The

*Corresponding Author: anil_aheciit@yahoo.com

DOI: 10.5098/hmt.11.33 ISSN: 2151-8629

investigational outcomes showed that the nanofluid flow boiling CHF was improved under the forced convective stream conditions compared to that in pure water.

Behnampour et al. (2017) examined the outcome of rectangular, triangular, and trapezoidal ribs on the average heat transfer of $H_2O - Ag$ nanofluid in a roughened triangular channel under a uniform heat flux. Among all of the investigated rib forms, heat transfer values are least for rectangular rib from and the triangular form has the best thermal performance. Hassan et al. (2016) numerical analysis is conducted to study the results of using nanofluids on impinging slot jet over a flat plate with a ribbed surface. Results indicated a marked improvement in average Nusselt number with the increase in the solid volume fraction. Vanaki and Mohammed (2015) examined the effect of dissimilar obstacle shapes and turbulent nanofluid flow on the efficiency factor through transversely ribbed rectangular ducts with flow parameter ranging from 5000 to 20000. It is found that the $SiO_2 - H_2O$ shows the highest heat transfer enhancement compared with other (Al_2O_3, CuO, SiO_2 and ZnO) tested nanofluids. The $\mathrm{Nu_{ave}}$ through the ribbed channels was enhanced with the increase of φ and $\mathrm{Re_n}$and with the decrease ofd_{np}.

Andreozzi et al. (2016) examined the effect of different rib shapes on heat transfer and $Al_2O_3 - H_2O$ nanofluid flow characteristics of a channel. Simulations for different φ from 0%, pure H_2O, to 4% and flow parameter between 20,000 and 60,000 are accomplished. They observed that, rectangular-trapezoidal-geometry rib highest efficiency factor at a pitch-rib-height equivalent to 10. Nassan et al. (2010) experimental studied Nu_{rs} and f_{rs} characteristics of $Al_2O_3 - H_2O$ and $CuO - H_2O$ nanofluids through a square channel in laminar flow under constant heat flux. Their results indicate that a considerable efficiency factor enhancement has been achieved by both nanofluids likened with base fluid.

Ahmed et al. (2015a) examined the Nu_{rs} and f_{rs} in an equilateral triangular channel using joint turbulence promoters and nanofluids. Both numerical and experimental results show a good enhancement in efficiency factor by using turbulence promoter with base fluid. Khoshvaght-Aliabadi et al. (2016) experimentally examined the performance of different metallic nanofluids on average heat transfer and flow friction mechanics in a pin rectangular channel. Their experimentations are performed using 0.1 % mass concentration of $Cu - H_2O$, $Fe - H_2O$, and $Ag - H_2O$nanofluids. Results indicate that the use of pins inside the duct can noticeably improve the heat transfer performance.

Al-Shamani et al. (2015) carried mathematical optimization of heat transfer due to turbulent flow of nanofluids over rib-groove duct. Their outcomes showed that the average Nusselt number rises as the volume fraction rises and it reductions as the nanoparticle diameter rises. Abdolbaqi et al. (2014) investigated the efficiency factor improvement of nanofluids under turbulent flow over a conventional square duct under uniform heat flux conditions at the upper and lower walls. The results show that the heat transfer rates and wall shear stress increase by increasing the nanofluids volume concentration. Zeinali Heris et al. (2007) experimentally examined the laminar stream forced convection heat transfer of $Al_2O_3 - H_2O$ nanofluid inside a ribbed tube with uniform wall temperature. Comparison of numerical data of ribbed tubes with plain tube shown that the heat transfer coefficient from 92% to 621% and friction factor from 25% to 241% compared to those obtained in smooth tube.

Wen and Ding (2004) determined that the efficiency factor of nanofluids, made of γ-Al_2O_3 nanoparticles and de-ionized water, flowing through a copper round tube in the laminar flow regime. Their results showed considerable improvement of efficiency factor by means of the nanofluids. Xu and Pop (2014) examined the fully developed mixed bioconvection current in a horizontal duct filled with a nanofluid that contains together nanoparticles and gyrotactic micro-organisms. Ahmed et al. (2012) indicate the $2D$-laminar flow of various nanofluids flow inside a triangular passage with the existence of turbulence promoter is numerically examined. Their results show that for the case of SiO_2 at $\varphi = 6\%$ and $Re = 800$, it is observed that the average heat transfer is about 50% better than the case of $Re = 100$.

Vatani and Mohammed (2013) investigated the effects of various rib-groove forms of arc, triangular and square, dissimilar geometrical parameters and also dissimilar types of nanofluids including Al_2O_3, CuO, ZnO and SiO_2 on the efficiency factor of stream in a horizontal obstacle-grooved duct are numerically examined. Their outcomes revealed that rectangular obstacle- rectangular groove shows the finest performance having the uppermost efficiency factor. Heyhat et al. (2012) examined the effect of Nu_{rs} and f_{rs} of the nanofluids in a round tube with uniform wall temperature under turbulent stream conditions experimentally. Parsazadeh et al. (2013) reported that the nanofluid flow is numerically examined to analyses the outcomes of numerous types of nanoparticles with numerous nanoparticle parameters in a fully detached obstacle roughened duct. The consequences indicate that the highest heat transfer enhancement is achieved with SiO_2 nanofluid and the flow friction not significantly change with by means of dissimilar types of nanoparticles in the base fluid. Vanaki et al. (2014) examined the outcomes of numerous nanofluids on the thermal and stream fields over transversely wavy wall passages with dissimilar phase shifts between the upper and lower wavy walls. Their results indicated that the wavy duct performance was importantly influenced by altering the phase shift and the wavy amplitude.

Ahmed et al. (2013) discussed the laminar turbulent heat transfer of $Cuo - H_2O$ nanofluid in trapezoidal-corrugated duct has been numerically examined. Their outcomes observed that the average Nu_{rs} improves with growth in nanoparticles volume fraction and with the amplitude of corrugated duct but this improvement accompanied by rises in flow friction. Ahmed et al. (2014) discussed the laminar forced convection stream of $Al_2O_3 - H_2O$ nanofluid in sinusoidal-curvy duct is numerically examined. Their outcomes that the numerical solution is obtained for flow parameter and nanoparticle fractions of volume ranges of 100-800 and 0-5%, respectively. Khdher et al. (2015) investigated experimentally and numerically the effect onNu_{rs} and f_{rs} for $Al_2O_3 - H_2O$ nanofluid flow inside circumferential roughened round tubes with various obstacle dimensions.

Manca et al. (2012) numerically studied the consequence hydrodynamic and thermal characteristics of turbulent nanofluids flow in a ribbed channel. Ahmed et al. (2015b) investigated experimentally the effect of nanofluid and turbulence promoter compound on average heat transfer and average friction factor in an equilateral triangular channel. Chokphoemphun et al. (2015) discussed the influence of winglet vortex generators placed in the core flow area on thermal performance enhancement of a tube heat exchanger. Their results observed that thermal performance for the winglet vortex generators is found to be much superior to that for the wire coil and twisted tape and is in a variety of 1.35-1.59. Mohammed et al. (2012) examined the consequence hydrodynamic and thermal characteristics of turbulent nanofluids flow in a rib-groove duct are numerically studied. Their results that the SiO_2 nanofluid has the supreme average heat transfer compared with other nanofluid types.

Haridas et al. (2015) presented a direct comparison of heat transfer characteristics of Al_2O_3 and SiO_2 nanoparticles on the basis of their relative influence on the thickness of thermal boundary layers, temperature gradients and the resultant heat transfer rates. The results of the study clearly reveal the effectiveness and higher heat transfer characteristics of Al_2O_3 nanoparticles than that of SiO_2 and experimentally demonstrated that the phenomena like increased thermal conductivity, boundary layer disruptions and advection effects primarily control the heat transfer rates in the lower range of Reynolds number.
Abed et al. (2015) numerically studied the fully developed turbulent flow and heat transfer behavior of Al_2O_3, CuO, SiO_2 and ZnOin trapezoidal channels using nanofluids with different volume fractions (0-4%) and diameters (20-80nm) under constant heat flux. The results indicated that SiO_2 has the highest Nusselt number among the nanofluids.

Global Digital Central
ISSN: 2151-8629

Enhancement of heat transfer increases with particle volume concentration, but a slight increase in pressure loss with decreasing nanoparticle diameter is also observed.

From this brief review [Navaei et al. (2015); Vanaki and Mohammed (2015); Al-Shamani et al. (2015); Parsazadeh et al. (2013); Vanaki et al. (2014); Ahmed et al. (2013); Manca et al. (2012); Mohammed et al. (2012); Haridas et al. (2015); Abed et al. (2015)] it follows that currently in the field of turbulent heat transfer of nanofluids there are still many unresolved issues. In particular, most of the works do not discuss in principle the issue of thermal-hydraulic efficiency of $TiO_2 - H_2O$ based nanofluid flow in V-pattern protruded rib square channel on heat transfer and flow friction. The current analysis has been taken up to explore the effect of concentration, particle diameter, protrusion rib size, protrusion rib height, print diameter of rib and angle of attack on the thermal and hydrodynamic ribbed square channel. Extensive experimentations have been conducted to generate data pertaining to heat transfer and flow friction for fully developed turbulent nanofluid flow through V-pattern protrusion square channel.

The main objectives of the present experimental analysis are:

- To investigate the effect of $TiO_2 - H_2O$ based nanofluid flow in V-pattern protruded rib square channel on heat transfer and flow friction.
- To find out superior thermal hydrodynamic performance of $TiO_2 - H_2O$ based nanofluid flow in V-pattern protruded rib square channel.
- To develop correlations for Nusselt number and flow friction of $TiO_2 - H_2O$ based nanofluid flow in V-pattern protruded rib square channel.

2. THERMO PHYSICAL PROPERTIES OF NANOFLUID

The following standard equations are used to compute density, specific heat, thermal conductivity and viscosity of the nanofluid.

The density of nanofluid is obtained by (Ho et al., 2008):

$$\rho_{nf} = (1-\varphi)\rho_{bf} + \varphi\rho_{np} \quad (1)$$

The specific heat of the nanofluid is obtained by (Ho et al. 2008):

$$(\rho C_p)_{nf} = (1-\varphi)(\rho C_p)_{bf} + \varphi(\rho C_p)_{np} \quad (2)$$

The effective thermal conductivity of the nanofluid is obtained by following correlations (Vajjha and Das 2009):

$$k_{eff} = k_{static} + k_{Brownian}$$

$$k_{static} = k_{bf}\left[\frac{(k_{np}+2k_{bf}) - 2\varphi(k_{bf}-k_{np})}{(k_{np}+2k_{bf}) + \varphi(k_{bf}-k_{np})}\right] \quad (3)$$

$$k_{Brownian} = 5\times10^4\beta\varphi\rho_{bf}C_{p,bf}\sqrt{\frac{KT}{2\rho_{np}R_{np}}}f(T,\varphi) \quad (4)$$

where $K(Boltzmann\ constant) = 1.3807\times10^{-23}J/K$, β represents the fraction of liquid volume which travels with particle and T is the temperature.

Modeling, $f(T,\varphi) = (2.8217\times10^{-2}\varphi + 3.917\times10^{-3})\left(\frac{T}{T_o}\right)$

$$+(-3.0669\times10^{-2}\varphi - 3.91123\times10^{-3}) \quad (5)$$

For $1\% \le \varphi \le 4\%$and $300K < T < 325K, T_0 = 293K$.

Thermophysical properties of nanoparticle and water are listed in Table.1.

Table.1 Thermophysical properties of nanoparticle and water.

Type of base fluid and nanoparticles	$\rho(kgm^{-3})$	$k(Wm^{-1}K^{-1})$	$C_p(Jkg^{-1}K^{-1})$	$\mu(Nsm^{-2})$
Water	998.20	0.613	4182	0.001003
TiO_2	3940	36.00	710	0.00102

3. PREPARATION OF NANOFLUID

Titanium oxide nanofluid preparation must ensure proper dispersion of nanoparticles in the liquid and proper mechanism is needed to attain the stability of the suspension against sedimentation. The size of nanoparticles is 20nm-80nm. The ultrasonic homogenizer, digital weighting machine, pH adjusted apparatus, Nanofluid ready flasks are depicted in Fig. 1 respectively. The digital weighting machine used in the present study is shown in Fig. 1(a). The nanoparticles and base fluid is mixed using mechanical stirrer and immersed in ultrasonic vibration as shown in Fig. 1(b) for 1.5 hours. After making the proper solid/liquid mixture, the flask was kept under ultrasonic vibration for 60 min and there was no sedimentation observed for long time (more than 140 hrs) and there after minor sedimentation was observed for 1 vol. % (1wt %) of TiO_2–water nanofluid only. The pH value of the base fluid water is adjusted with the addition of small amount of hydrochloric acid. The pH meter used in the present study is shown in Fig. 1(c). The prepared nanofluid flasks are shown in Fig.1(d). The unknown weight of the nano powder is estimated based on the known percentage of volume fraction, density of the particle and density of the water by law of mixtures.

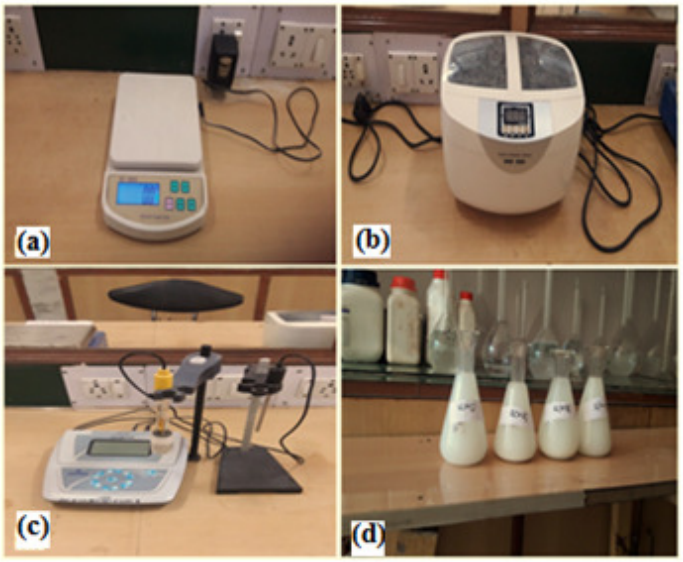

Fig. 1 Photographic view (a) Digital weighting machine (b) Ultrasonic homogenizer (c) pH adjusted machine (d) Nanofluid prepared flasks.

4. ROUGHNESS PARAMETERS

In current experimental analysis the $TiO_2 - H_2O$ based nanofluid flow in V-type protruded rib square channel is selected; channel width (W_C)=10mm, channel height (H_C)=10mm and total length of channel is 340 mm. The length of test section is $L_t = 108\,mm$. The results are formed on square channel with V-type protruded obstacle having four values of volume fraction(φ), four values of particle diameter (n_p), four values of relative V-pattern protruded- rib height (H_d/D_h), four values of ratio of V-pattern protruded height-to-print diameter(H_d/d_p), four values of relative V-pattern protruded rib pitch (P_d/H_d) and four values of angle-of-attack (α_a) respectively. The profile and photographic view of V-type protruded ribs are depicted in Fig. 2 respectively. The values and ranges of variant experimental ribbed parameters are presented in Table 2.

5. EXPERIMENTAL SETUP

To analysis the results of V-pattern protruded obstacle square duct on the Nu_{rs} and f_{rs} of air stream an experimental setup was intended and made-up accordance with guidelines recommended in ASHRAE standard (Lehtimaki et al. 2002). A schematic diagram of experimental setup is presented in Fig. 3. The experimental arrangement consists of a test

Global Digital Central
ISSN: 2151-8629

section with installed heater, a control panel, a collecting tank, a circulating pump, a condenser (cooling unit).

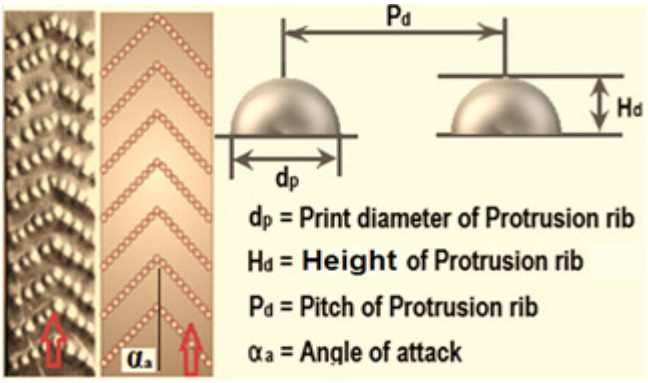

Fig. 2 Discuss V-type protrusion rib shape parameters.

Table.2 Range of experimental parameters.

Sr. No.	Parameters	Range
1.	φ	1 –4%
2.	n_p	30 – 45nm
3.	H_d/D_h	0.10 – 0.25
4.	H_d/d_p	0.8 – 2.0
5.	P_d/H_d	2 – 3.5
6.	α_a	$30^0 – 75^0$
7.	Re	4000-8000

The length of test section is $L_t = 108\ mm$, with an upstream length of $200\ mm$ to confirm a fully developed stream in the test unit. The fluid was forced to the developing unit and then to the test unit in order to get a fully developed stream before incoming the test unit. The entrance unit ensures a hydro dynamically developed stream before incoming the test unit. A fixed heat flux of 10 kW/m^2 is provided with the support of Nicrome wire as heating elements and variac transformer. T-category thermocouple was used to calculate the temperature reading with the support of data loggers. Seven thermocouples were used, out of which four were located on heated wall, one at inlet and two at the exit. The nanofluid fluid was forced to the developing unit and then to the test unit in order to get a fully developed stream before inflowing the test unit. A switch panel was arranged as the main connector of the scheme to the power supply. The pressure losses over the square heat exchanger duct developed was determined by a U-tube manometer. Submersible pump was used to drive the employed fluid from tank of 10- litre capacity to stream through the test unit. Electrical heater plate was used to heat the top surface of the test unit. The electrical heater was connected to AC power regulator unit which was used to control the input voltage and current to the heaters. A flow meter was linked between the pump and the inlet of the developing unit to calculate the mass flow rate of the fluid. A cooler with $1kW$ cooling capacity was immersed inside the tank to adjust the temperature of the working fluid enters the test section. Before consecutively each experimentation, enormous cautions were taken to insure suitable performance of entire test setup and there was no leakage at joints in experimental setup. The similar devices propose the consequences under steady states which were expected to be attained while there was no substantial variation in nanofluid flow duct and roughened plate temperature was noted above duration of more than 15 min.

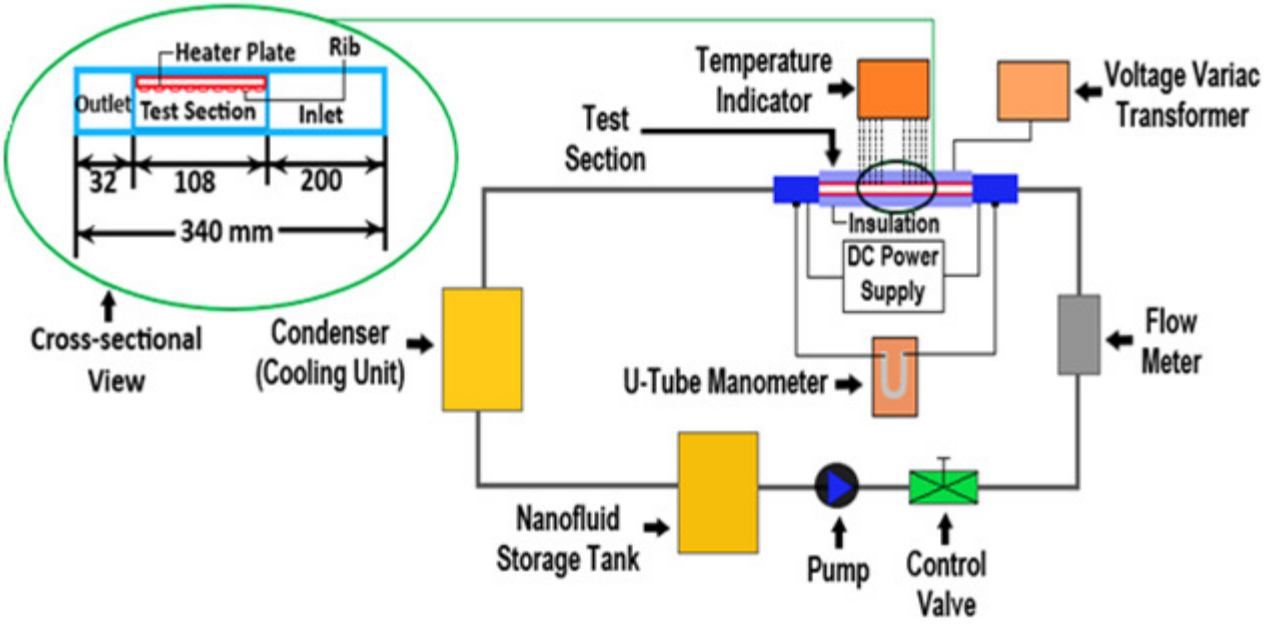

Fig. 3 Schematic diagram of experimental setup.

6. DATA REDUCTION

Raw data collected by experimentation are used to estimate the values of dimensionless numbers like Reynolds number (Re), Nusselt number (Nu_{rs}), friction factor (f_{rs}), hydraulic diameter (D_h), heat transfer coefficient (h_c) and thermal hydrodynamic performance (η_p) have been determined by employing the following equations as depicted below:
The Re is calculating as:

$$Re = \frac{\rho_{nf}.v_x.d_H}{\mu_{nf}} \quad (6)$$

Here, D_h is determined as follow:

$$D_h = \frac{4.W_c.H_c}{2.(W_c + H_c)} \quad (7)$$

The Nu_{rs} is determined as:

Global Digital Central
ISSN: 2151-8629

$$Nu_{rs} = \frac{h_c . L_t}{k_{nf}} \quad (8)$$

where k_{nf} is the thermal conductivity of nanofluid.
Here, h_c is determined as:

$$h_c = \frac{Q}{A_p . (T_{pt} - T_{ft})} \quad (9)$$

Here, T_{pt} is the area of weighted average plate temperature and T_{ft} is the average fluid temperature respectively.
The f_{rs} is calculated as:

$$f_{rs} = \frac{2\Delta P D_h}{\rho_{nf} L_t {v_x}^2} \quad (10)$$

The $\eta_p$is determined as:

$$\eta_p = \frac{\left(\frac{Nu_{rs}}{Nu_{ss}}\right)}{\left(\frac{f_{rs}}{f_{ss}}\right)^{1/3}} \quad (11)$$

7. VALIDATION OF EXPERIMENTAL SETUP

The results of Nu_{ss} and f_{ss} collected from experimental designs for plain square channel has been compared among the results obtained from the Gnielinski correlation equation for Nu_{ss} depicted in equation (12) and Petukhov correlation equation for f_{ss} depicted in equation (13) respectively.

The Nu_{ss} for smooth wall square duct is obtainable by using Gnielinski correlation equation as follow:

$$Nu_{ss} = \frac{\left(\frac{f_{rs}}{8}\right)(Re - 1000)Pr^{0.4}}{1 + 12.7\left(\frac{f_{ss}}{8}\right)^{\frac{1}{2}}\left(Pr^{\frac{2}{3}} - 1\right)} \quad for\ 3{,}000 \le Re \le 21{,}000 \quad (12)$$

The f_{ss} for smooth wall square channel is obtainable by using Petukhov correlation equation as follow:

$$f_{ss} = (0.079 ln Re - 1.64)^{-2} \quad (13)$$

The intended results of experimental and predicted outcomes of Nu_{ss} and f_{ss} as a function of Re is presented in Figs. 4 and 5 respectively. In order to show the variation of Nu_{ss} and f_{ss} as a function of Reynolds number the error bars are drawn and shown in Figs. 6 and 7. The average absolute deviation among experimental and predicted values of Nu_{ss} and f_{ss} has been found to be 4.38% and 3.19% respectively. This resonably good accuracy among the two sets of values, confirms the correctness of the data being arranged using this experimental setup.

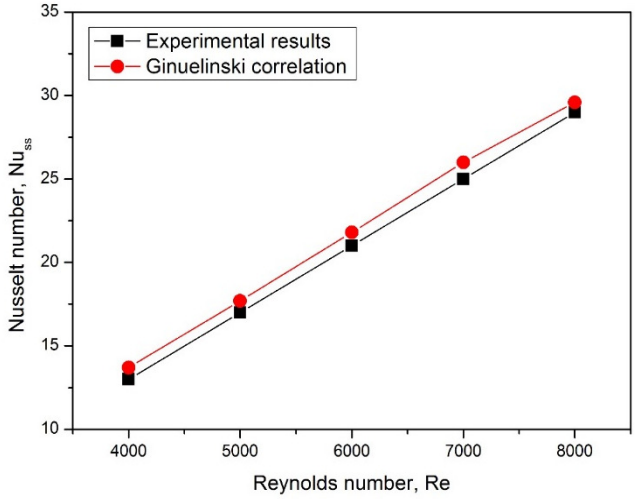

Fig. 4 Comparison of experimental and predicted values of Nu_{ss} for smooth surface square channel.

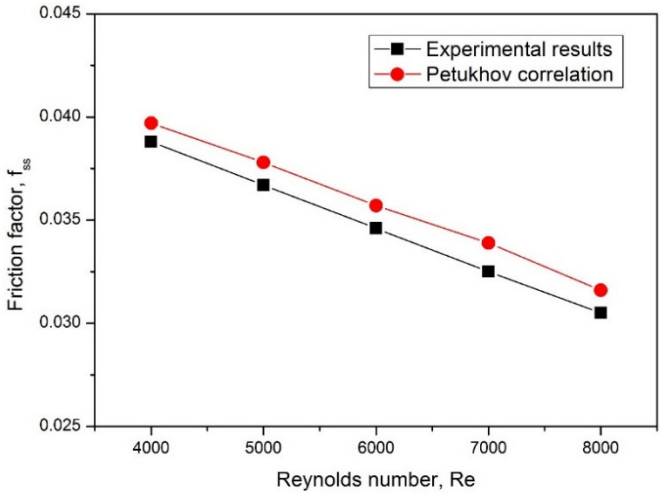

Fig. 5 Comparison of experimental and predicted values of f_{ss} for smooth surface square channel.

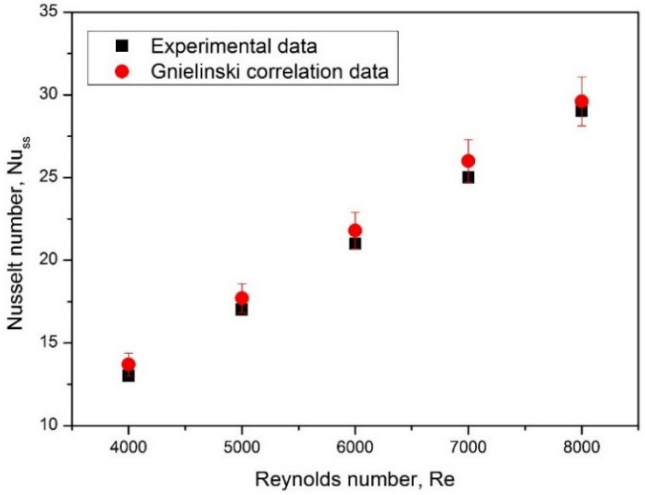

Fig. 6 Error bar analysis of smooth surface square channel for Nusselt number.

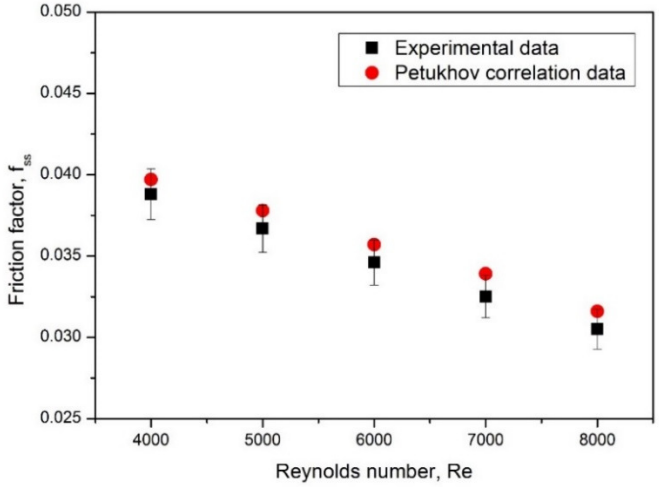

Fig. 7 Error bar analysis of smooth surface square channel for friction factor.

Global Digital Central
ISSN: 2151-8629

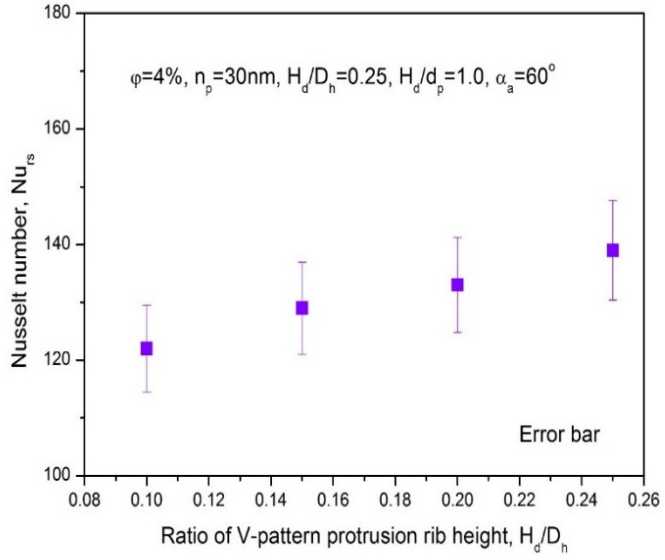

Fig. 8 Error bar analysis of V-pattern protrusion rib for Nusselt number.

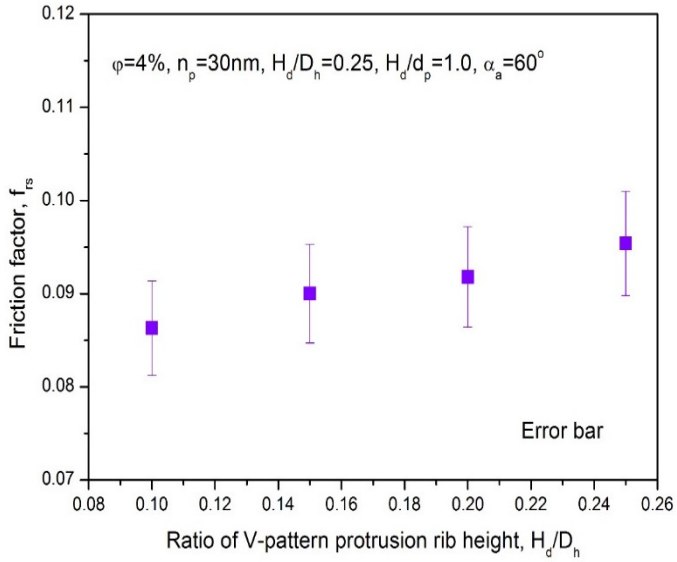

Fig. 9 Error bar analysis of V-pattern protrusion rib for friction factor.

8. UNCERTAINTY ANALYSIS

The measurement uncertainty of various important quantities has been evaluated (Coleman and Steele 2009) and is in control limits. The procedure for computation of uncertainty is discussed below:

The uncertainty in measurement of "y" when the parameter is calculated using specific measured quantities is given by:

$$\frac{\delta y}{y}=\left[\left(\frac{\delta y}{\delta x_1}\delta x_1\right)^2+\left(\frac{\delta y}{\delta x_2}\delta x_2\right)^2+\left(\frac{\delta y}{\delta x_3}\delta x_3\right)^2+\cdots+\left(\frac{\delta y}{\delta x_n}\delta x_n\right)^2\right]^{0.5} \quad (14)$$

where, δx_1,δx_2,δx_3, …. δx_n are the possible error in measurement of x_1,x_2, x_3, …..x_n.

$\delta_y$is absolute uncertainty and $\frac{\delta_y}{y}$ the relative uncertainty.

Uncertainty in area of heated plate (A_p)

$$A_p = W_c \times L_t \quad (15)$$

$$A_p=\left[\left(\frac{\delta A_p}{\delta L_t}L_t\right)^2+\left(\frac{\delta A_p}{\delta W_c}\delta W_c\right)^2\right]^{0.5} \quad (16)$$

$$\frac{\delta A_p}{A_p}=\left[\left(\frac{\delta L_t}{L_t}\right)^2+\left(\frac{\delta W_c}{W_c}\right)^2\right]^{0.5} \quad (17)$$

Uncertainty in area of flow (A_f)

$$A_f = W_c \times H_c \quad (18)$$

$$A_f=\left[\left(\frac{\delta A_f}{\delta W_c}\delta W_c\right)^2+\left(\frac{\delta A_f}{\delta H_c}\delta H_c\right)^2\right]^{0.5} \quad (19)$$

$$\frac{\delta A_f}{A_f}=\left[\left(\frac{W_c\times\delta H_c}{W_c\times H_c}\right)^2+\left(\frac{H_c\times\delta W_c}{W_c\times H_c}\right)^2\right]^{0.5} \quad (20)$$

Uncertainty in measurement of Hydraulic diameter (D_h)

$$D_h=\frac{4\times(W_c\times H_c)}{2\times(W_c\times H_c)}=2(W_cH_c)(W_c+H_c)^{-2} \quad (21)$$

$$\frac{\delta D_h}{\delta H_c}=[2(W_cH_c)(-1)(W_c+H_c)^{-2}]+[(W_c+H_c)^{-1}(2W_c)] \quad (22)$$

Uncertainty in useful heat gain (Q_u)

$$Q_u = m_a c_p \Delta T \quad (23)$$

$$\frac{\delta Q_u}{Q_u}=\left[\left(\frac{\delta m_a}{m_a}\right)^2+\left(\frac{\delta c_p}{c_p}\right)^2+\left(\frac{\delta\Delta T}{\Delta T}\right)^2\right]^{0.5} \quad (24)$$

Uncertainty in heat transfer coefficient (h_t)

$$h_c=\frac{Q_u}{A_p.(T_{pt}-T_{ft})}=\frac{Q_u}{A_p\times\Delta T_f} \quad (25)$$

$$\frac{\delta h_c}{h_c}=\left[\left(\frac{\delta Q_u}{Q_u}\right)^2+\left(\frac{\delta A_p}{A_p}\right)^2+\left(\frac{\delta\Delta T_f}{\Delta T_f}\right)^2\right]^{0.5} \quad (26)$$

Uncertainty in Nusselt number (Nu_{rs})

$$Nu_{rs}=\frac{h_c.L_t}{k_{nf}} \quad (27)$$

$$\frac{\delta Nu_{rs}}{Nu_{rs}}=\left[\left(\frac{\delta D_h}{D_h}\right)^2+\left(\frac{\delta h_c}{h_c}\right)^2+\left(\frac{\delta k_{nf}}{k_{nf}}\right)^2\right]^{0.5} \quad (28)$$

Uncertainty in Reynolds Number (Re)

$$Re=\frac{\rho_{nf}.v_x.D_h}{\mu_{nf}} \quad (29)$$

$$\frac{\delta Re}{Re}=\left[\left(\frac{\delta D_h}{D_h}\right)^2+\left(\frac{\delta v_x}{v_x}\right)^2+\left(\frac{\delta\rho_{nf}}{\rho_{nf}}\right)^2+\left(\frac{\delta\mu_{nf}}{\mu_{nf}}\right)^2\right]^{0.5} \quad (30)$$

Uncertainty in friction factor (f_{rs})

$$f_{rs}=\frac{2\Delta P_0 D_h}{\rho_{nf}L_t{v_x}^2} \quad (31)$$

$$\frac{\delta f_{rs}}{f_{rs}}=\left[\left(\frac{\delta D_h}{D_h}\right)^2+\left(\frac{\delta v_x}{v_x}\right)^2+\left(\frac{\delta L_t}{L_t}\right)^2+\left(\frac{\delta\rho_{nf}}{\rho_{nf}}\right)^2+\left(\frac{\delta\Delta P_0}{\delta\Delta P_0}\right)^2\right]^{0.5} \quad (32)$$

Uncertainty in thermal hydraulic performance parameter (η_p)

$$\eta_p=\frac{\frac{Nu_{rs}}{Nu_{ss}}}{\left(\frac{f_{rs}}{f_{ss}}\right)^{0.33}} \quad (33)$$

$$\frac{\delta\eta_p}{\eta_p}=\left[\left(\frac{\delta Nu_{rs}}{Nu_{rs}}\right)^2+\left(\frac{\delta f_{rs}}{f_{rs}}\right)^2\right]^{0.5} \quad (34)$$

Based on the examined of the errors in the experimental measurements using different instruments, the uncertainties in the calculated value of Nusselt number and friction factor have been estimated as $\pm 6.18\%$ and $\pm 5.89\%$, respectively. The variation of Nusselt number and friction factor as a function of ratio of V-pattern

Global Digital Central
ISSN: 2151-8629

protrusion rib height the error bars are drawn and shown in Figs. 8 and 9.

9. RESULTS AND DISCUSSIONS

The consequence of V-pattern protruded rib and flow parameters on heat transfer rates to the $TiO_2 - H_2O$ based nanofluid with square channel is discussed in this section. The consequence of V-pattern protruded rib profile on heat transfer and pressure drop has been presented for dissimilar factors like φ, n_p, H_d/D_h, H_d/d_p, P_d/H_d and α_a.

9.1 HEAT TRANSFER AND FLUID FLOW

The schemes for Nusselt number as significance φ for dissimilar values of Re are depicted in Fig. 10(a) and the remaining parameters are constant such as; $n_p = 30$, $H_d/D_h = 0.25$, $H_d/d_p = 1.0$, $P_d/H_d = 2.5$ and $\alpha_a = 60^0$. The above graph depicts that Nu_{rs} increased due to increase in φ from 1.0% to 4.0% and attains the maximum resultant values at φ = 4%, and after that enhancement the data plotted in graph starts to decrease. It has been found that in each data of φ the V-type protruded obstacle wall generates superior heat transfer than that of without V-type protruded obstacle surface square duct.

The secondary stream has two variant types of revolving vortices which transmits the cold nano fluid from inner central part region to the protrusion among V-pattern protruded obstacle wall and these streams combined among the major stream. Such internal flow $TiO_2 - H_2O$ based nano fluid mixed among the inner flow, effect stream reconnection and retransmission within the V-pattern protruded obstacle and the suspended boundary conditions a developed to the downstream of reattachment regions. When Re raised the width of boundary layer reduced due to reduction in convective resistance and hence Nu_{rs} is enhanced correspondingly. The V-type protrusion ribs produce a strong secondary stream at the back of limbs and sustains the turbulence accumulation while $TiO_2 - H_2O$ nano fluid detach from single V-shape protrusion ribs and mixing with the main flow. The effect of Nu_{rs} with Re for variant data of n_p is presented in Fig. 10 (b). The values of other roughness parameters are fixed such as; φ = 4.0%, H_d/D_h = 0.25, H_d/d_p = 1, P_d/H_d = 2.5 and $\alpha_a = 60^0$. It is obtained that Nu_{rs} raises with raise in the data of n_p for every value of Re due to the expanded flow velocity which is directed to maximum turbulence, hence resulting an enhancement in Nu_{rs}. Fig. 10(c) demonstrations the variation of Nusselt number as a function of Re for different data H_d/D_h and the values of other roughness parameters are kept such as φ = 4.0%, n_p = 30, H_d/d_p = 1.0, P_d/H_d = 2.5 and $\alpha_a = 60^0$.

It is clearly seen that the Nu_{rs} increase with increase in H_d/D_h. It is believed that an artificial roughness on the heat transfer surface in the form of V-pattern protrusion rib creates local wall turbulence or breaks the laminar sub layer due to flow separation and reattachment between the consecutive ribs, which reduces thermal resistance and greatly enhance rate of heat transfer. For each Re, the highest results of Nu_{rs} are achieved at H_d/D_h = 0.25, whereas the smaller resultant values of Nu_{rs} are realised to occur at H_d/D_h = 0.10 for the range of parameters investigated. Maximum enhancement in the heat transfer of four times as compared to a smooth plate is observed for the H_d/D_h value of 0.25 at Re of 8,000.

The deviations of Nu_{rs} as a function of Re for variant values of H_d/d_p are showed in Fig. 10(d). The remaining experimental factors like φ = 4%, n_p = 30, $H_d/D_h = 0.25$, P_d/H_d = 2.5 and $\alpha_a = 60^0$ are fixed. The above graph depicts that Nu_{rs} increases with increase in the values of H_d/d_p for all data of Re due to elevated flow which is prone to highest turbulence, therefore providing an optimal increase in Nu_{rs}. The maximum Nu_{rs} is achieved at H_d/d_p = 1.0, after this enhancement in Nu_{rs} it begins to reduce with increase in the data of H_d/d_p and least value of Nu_{rs} is obtained at H_d/d_p = 2.0 respectively.

The Nu_{rs} is observed for increase in H_d/d_p from 0.8 to 1.0, however, Nusselt number increased considerably for H_d/d_p value of 1.0 and decreased for further increase in the value to 1.3. Further increase in the H_d/d_p value to 1.3, causes decrease in Nusselt number values. This may be due to the fact that for ratio of V-pattern protrusion height to print diameter values much more than the thickness of the laminar sublayer, increase in the turbulence is more prominent in the core flow rather than within the boundary layer, which is not much beneficial for enhancing the convective heat transfer from the heated plate. Maximum enhancement in the heat transfer of four times as compared to a smooth plate is observed for the H_d/d_p value of 1.0 at Re of 8,000.

The dissimilarity of Nu_{rs} as a meaning of Re for different data of P_d/H_d are presented in Fig. 10(e). The values of other roughness parameters are fixed such as φ = 4%, n_p = 30, $H_d/D_h = 0.25$, $H_d/d_p =$ 1.0 and $\alpha_a = 60^0$. The above plot depicts that Nu_{rs} rise due to rise the value of P_d/H_d and attain a maximum at $P_d/H_d = 2.5$, and after that rise the value plotted in graph starts to decrease. It can be seen that from graph the Nu_{rs} attain maxima corresponding to $P_d/H_d = 2.5$ and on either side of this value, decrease in Nu_{rs} has been observed. Maximum heat transfer has been found to occur in the vicinity on a reattachment point. It is reasonable to expect that a similar effect can be produced by decreasing P_d/H_d for a fixed value of relative roughness height. For P_d/H_d value considerably less than about 2.5, the reattachment will not occur at all resultant in the decrease of heat transfer enhancement.

For higher values of $P_d/H_d = 3.0$ and 3.5, Nu_{rs} value starts to decline sharply, because number of roughness elements becomes very less at these pitch values and hence overall number of reattachment points decreases. Higher pitch values also allow nanofluid to move longer after reattachment till it encounters the next rib and thereby leading to re-development of the laminar sublayer on some portion of the heated plate surface. Re-development of boundary layer adversely affects the heat transfer from the heated plate and hence decrease the heat transfer rate.

Fig. 10(f) demonstrations the variation of Nu_{rs} with Re for different data of α_a and the other V-pattern combined with protruded rib parameter fixed such as φ = 4%,n_p = 30,$H_d/D_h = 0.25$, $H_d/d_p = 1.0$ and P_d/H_d = 2.5 respectively. The Nu_{rs} raises because of the rise in α_a and attains the uppermost value correspondent to flow attack angle of 60^0, and after that increment it decreases due to increase in the data of α_a. From graph at all Re, the highest heat transfer is observed at $\alpha_a = 60^0$, and it reduces on both sides of this value. This variation in Nu_{rs} is caused by interaction of secondary flow along the V-pattern protrusion rib and boundary layer on upstream side of the V-pattern rib. The boundary layer is done to main flow with the roughened surface and originates from flow reattachment point between the ribs up to the succeeding downstream rib. The strength of secondary flow along the rib changes with change in values of flow attack angle. For the present study, the value of Nu_{rs} has been observed to be highest at $\alpha_a = 60^0$.

Application of V-pattern combined with protrusion rib roughness is supposed to result in more complicated flow patterns near the wall as shown in Fig. 11. It is believed that the flow patterns responsible for the enhancement of heat transfer are 1) reattachment of the primary flow behind the V-pattern protrusion rib 2) acceleration of the primary flow through the protrusions. 3) generation of the counter rotating secondary flow vortices across the cross section of the square duct. Relative contribution of these factors towards the heat transfer improvement depends upon the geometrical parameters of the V-pattern protrusion rib roughness.

On the other hand, presence of the recirculation region behind the V-pattern protrusion rib lowers the heat transfer from the heated plate. Shaping of an extended-inclined rib into V-type obstacle helps in the creation of two leading ends (where heat transfer rate is high) and a single trailing end (where heat transfer rate is low) resultant in much larger increase of heat transfer. V-shaped ribs form two secondary stream cells as compared to one in case of an inclined rib resultant in higher efficiency factor in case of V-shaped rib as shown in Fig. 11.

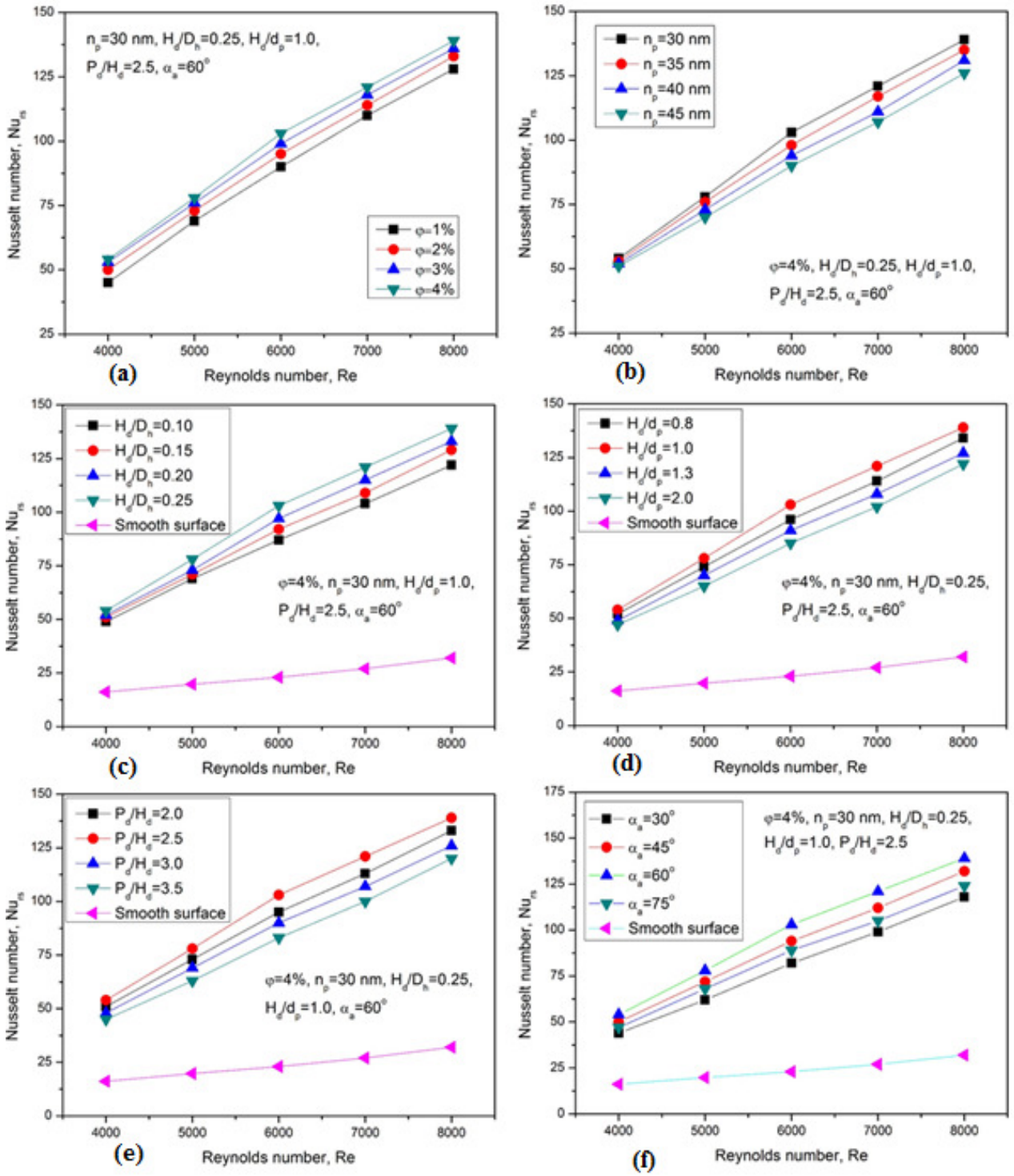

Fig. 10 (a) Effect of φ on Nu_{rs} (b) Effect of n_p on Nu_{rs} (c) Effect of H_d/D_h on Nu_{rs} (d) Effect of H_d/d_p on Nu_{rs} (e) Effect of P_d/H_d on Nu_{rs} (f) Effect of α_a on Nu_{rs}.

The roughness applied in the form of V-type protrusion ribs on a heated surface significantly improves Nu_{rs} from the excited surface of V-type $TiO_2 - H_2O$ based nano fluid square channel; however a significant increment takes place in f_{rs} losses. In the present experimental examination, it has been found that how f_{rs} characteristics of $TiO_2 - H_2O$ nano fluid square channel were effected while V-type protrusion ribs roughness parameter φ was varied and operating parameters are constant $n_p = 30$, $H_d/D_h = 0.25, H_d/d_p = 1.0$ and $P_d/H_d = 2.5$ and $\alpha_a = 60^0$ were reserved constant as shown in Fig. 12(a). The plot depicts that f_{rs} alters among Re for different data of φ and hence f_{rs} improves with decrease in Re for each case. With raise in φ the data of f_{rs} increases and obtains a highest value like φ value of 4% in the range of operating parameters. Several of the vortices increases the mixing of $TiO_2 - H_2O$ nano fluid and because of this Nu_{rs} enhanced. So, the Nu_{rs} increases from the target plate to nano fluid and these vortices also improve the highest Nu_{rs} during stream across the nano

Global Digital Central
ISSN: 2151-8629

fluid mini square passage. The quantity of vortices is higher in case of φ = 4% as compared to φ = 3%. Therefore, in case of φ = 4% $TiO_2 - H_2O$nano fluid and vortices mixing is higher, that gives a highest f_{rs}. The variation of f_{rs} with Re for different data of n_p has been presented in Fig. 12(b). The remaining rib roughness parameters like φ = 4%, H_d/D_h = 0.25, H_d/d_p = 1.0, P_d/H_d = 3.5 and α_a = 60° are fixed. It can be observed that f_{rs} rises with rise in n_p and the highest rate of f_{rs} correspondent to $n_p$will be equal to 30. The reason behind this is that due to rise in range of n_p, the $TiO_2 - H_2O$nano fluid spread out up to a huge area into the core of stream, results an enhancement in the data of f_{rs}. Fig. 12(c) presents the effect of Re on f_{rs} for various values of H_d/D_h. The remaining rib roughness parameters like φ = 4%,n_p = 30, H_d/d_p = 1.0, P_d/H_d = 2.5 and α_a = 60° are fixed. It has been observed that the highest value of f_{rs} at H_d/D_h = 0.25 and least value of f_{rs} at H_d/D_h = 0.10.

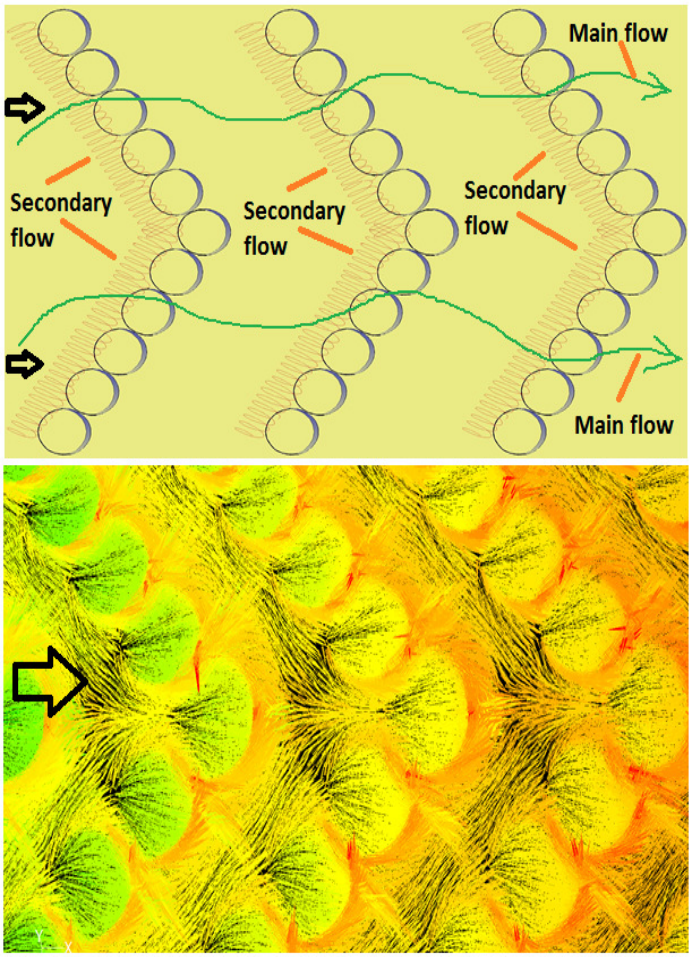

Fig. 11 Secondary flow pattern in V-type protruded ribbed square channel.

The distinction of $f_{rs}$with Re for different value of H_d/d_p is presented in Fig. 12(d) and the remaining of the roughness parameters like φ = 4%, n_p = 30, H_d/D_h = 0.25, P_d/H_d = 2.5 and α_a = 60^0 were constant. It clearly shows that for individual value of H_d/d_p, f_{rs} increases and the highest value for f_{rs} correspondent to $H_d/d_p$was achieved at a value of 1.0. It may be noted that friction factor trends exactly complement the trend of Nusselt number i.e., Nusselt number is high when turbulence level in the flow is high and increase in turbulence increases the friction factor. Friction is low at H_d/d_p value of 2.0 since proper flow reattachment does not take place at such a low rib height (with increase protrusion rib print diameter) of nanofluid flow over the ribs with low separation and reattachment between the upstream and downstream V-pattern protrusion rib. Flow friction increases sharply at H_d/d_p value of 1.0 due to increase in turbulence owing to the onset of separation-reattachment flow pattern.

Fig. 12(e) depicted the characteristics of f_{rs} with Re for different data P_d/H_d and the rib roughness parameters such as φ = 4%, n_p = 30, H_d/D_h = 0.25, H_d/d_p = 1.0 and α_a = 60^0 were fixed. It depicts that for individual value of P_d/H_d, f_{rs} increases and the highest value for f_{rs} correspondent to P_d/H_d was achieved at a value of 2.5. It may be noted that friction factor trends exactly complement the trend of Nusselt number i.e., Nusselt number is high when turbulence level in the flow is high and increase in turbulence increases the friction factor. Friction is low at P_d/H_d value of 2.0, since proper flow reattachment does not take place at such a low value of P_d/H_d and nanofluid flows over the ribs without touching the heated plate between the upstream and downstream ribs. Flow friction increases sharply at P_d/H_d value of 2.5 due to increase turbulence owing to the onset of separation-reattachment flow pattern. For P_d/H_d values of 3.0 and 3.5 flow friction decreases due to decrease in the number of roughness elements per unit length of the heated plate. Further increase in the P_d/H_d value of 3.0 and 3.5 results in the drop-in friction factor, because of decrease in the number of roughness elements per unit length of heated plate start dominating the influence of the V-pattern protrusion ribs hence friction factor start decreasing.

The difference of f_{rs} with Re for different data of $\alpha_a$and remaining of the roughness parameters like φ = 4%, n_p = 30, H_d/D_h = 0.25, H_d/d_p = 1.0 and P_d/H_d = 2.5 were kept as shown in Fig. 12(f). It has been obtained that for each value of α_a, f_{rs} reduces due to rise in Re and an enhancement is observed in f_{rs} at a value of α_a =60^0, however after this increment it begins to decrease with rise in α_a and attains highest possible data correspondent to α_a of 60^0.

It is believed that the combined effect of all the other fixed geometry parameters contributes toward the favorable effect of the secondary flows along the V-pattern with combined protrusion rib for better mixing and fast heat transfer for α_a of 60^0. Further increase in the V-pattern rib inclination to 75^0 results in considerable decrease in the strength of secondary flow vortices moving along the V-pattern protrusion ribs, because rib inclination approaches 90^0 for which vortices behind the rib becomes almost stationary leading to decrease in the friction factor.

9.2 THERMAL HYDRODYNAMIC PERFORMANCE

Experimental outcomes pertinent to protruded with combined V-pattern roughness shapes for the present analysis manifest significant enhancement in heat transfer rates with corresponding rise in pressure drop. To accomplish such function of concurrent consideration of η_p, (Webb and Eckert 1972) presents a thermal hydrodynamic performance parameters η_p deciding the Nu_{rs} via φ, n_p , H_d/D_h, H_d/d_p, P_d/H_d and α_a of V-pattern protruded ribs per unit propelling power estimated among Nu_{rs} for the perfectly formed turbulent stream in the passage among smooth features are presented as follow:

$$\eta_P = (Nu_{rs}/Nu_{ss})/(f_{rs}/f_{ss})^{0.33} \quad (35)$$

Fig.13(a-d) indicates the effect of protruded with combined V-pattern rib parameters on $(Nu_{rs}/Nu_{ss})/(f_{rs}/f_{ss})^{0.33}$ as a function of Re. The value of protruded rib with combined V-pattern surface factors in which $(Nu_{rs}/Nu_{ss})/(f_{rs}/f_{ss})^{0.33}$ values were achieved to be supreme is depicted in Fig.13. The uppermost outcomes of $(Nu_{rs}/Nu_{ss})/(f_{rs}/f_{ss})^{0.33}$ are attained to be 3.21 corresponding to φ = 4%, n_p = 30, H_d/D_h = 0.25, H_d/d_p = 1.0, P_d/H_d = 2.5 and α_a = 60^0 for whole value of Re selected for current examination. The greatest results of thermal hydrodynamic performance parameter for different factors are represents in Table.3.

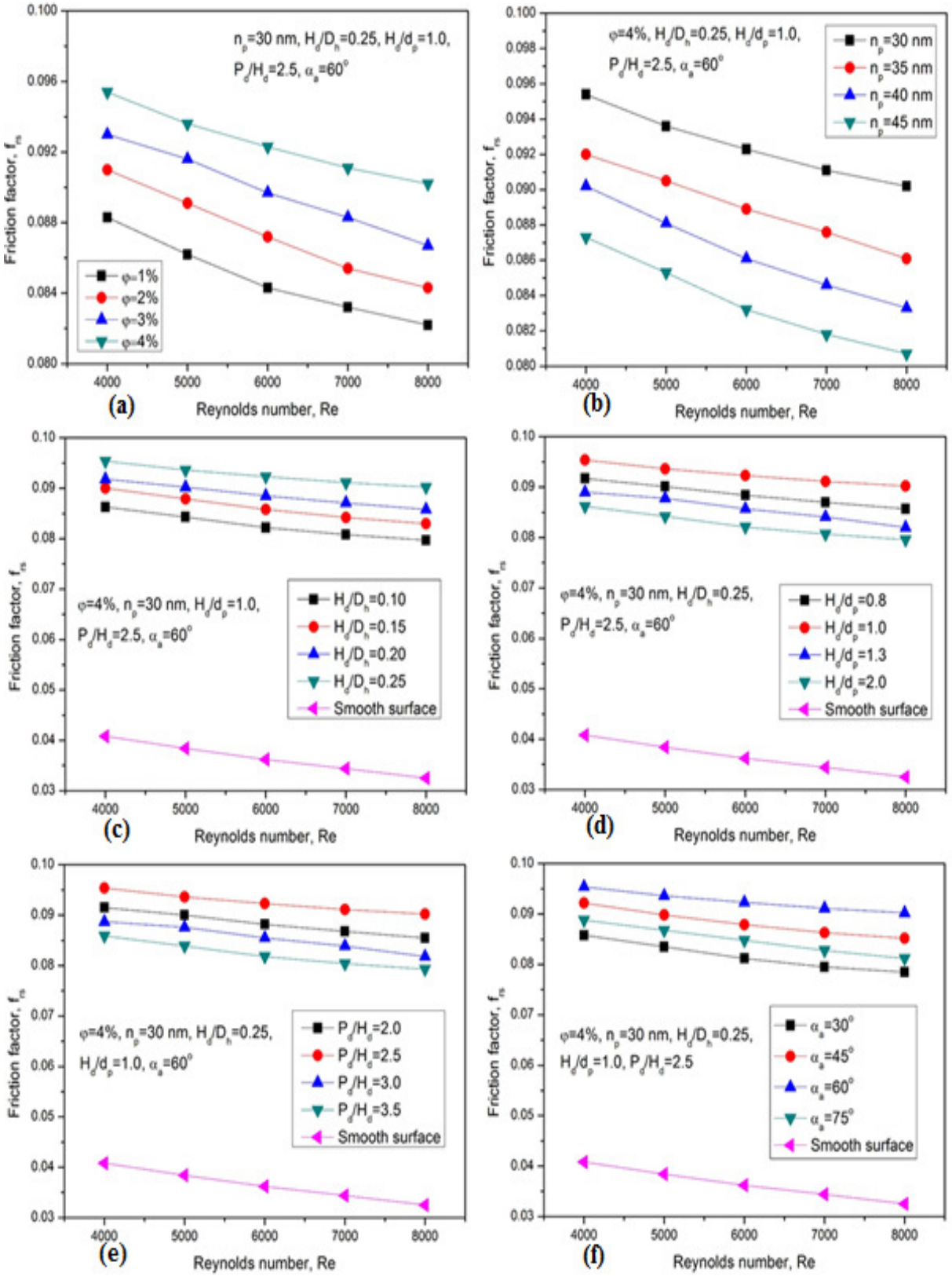

Fig. 12 (a) Effect of φ on f_{rs} (b) Effect of n_p on f_{rs} (c) Effect of H_d/D_h on f_{rs} (d) Effect of H_d/d_p on f_{rs} (e) Effect of P_d/H_d on f_{rs} (f) Effect of α_a on f_{rs}.

Global Digital Central
ISSN: 2151-8629

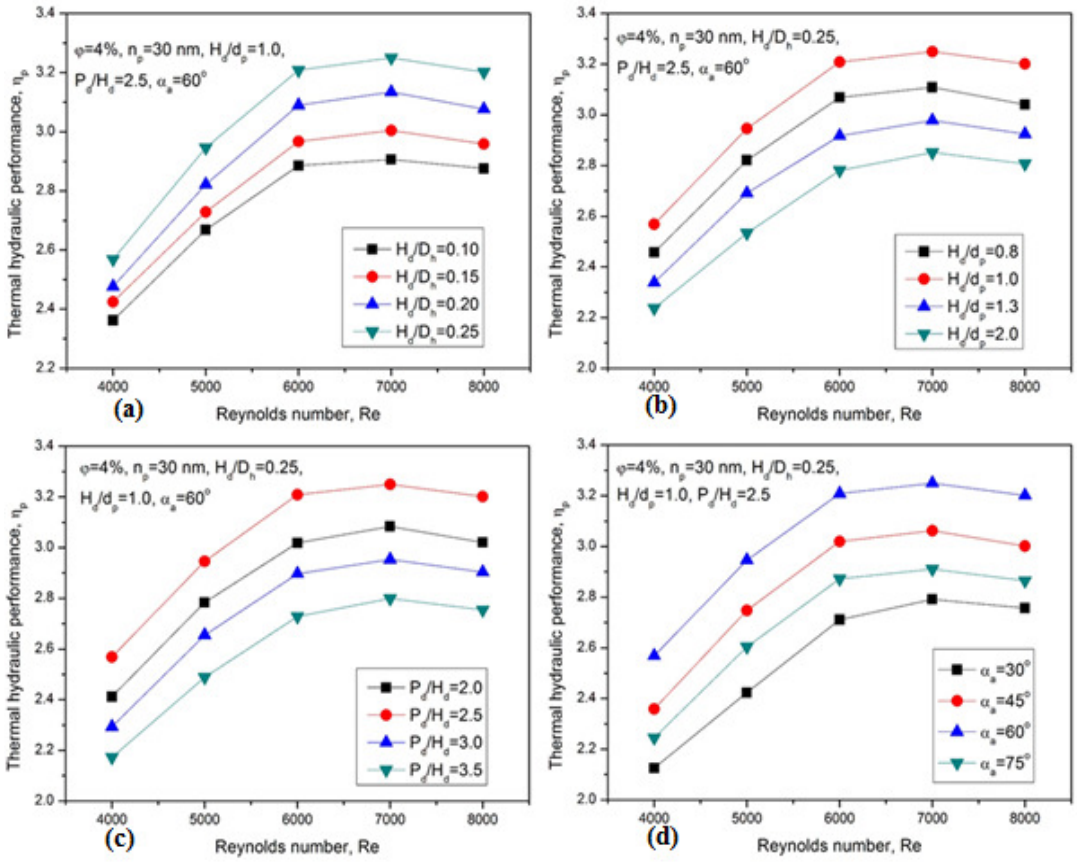

Fig. 13 (a) Effect of H_d/D_h on η_p(b) Effect of H_d/d_p on η_p (c) Effect of P_d/H_d on η_p(d) Effect of α_a on η_p.

Table. 3 V-type protruded rib parameter corresponding to maximum of $\eta_p = (Nu_{rs}/Nu_{ss})/(f_{rs}/f_{ss})^{0.33}$.

Sr. No.	Fixed parameters	Varied parameter	Thermal hydrodynamic performance
1.	$\varphi = 4\%, n_p = 30$, $H_d/d_p = 1.0$, $P_d/H_d = 2.5$ and $\alpha_a = 60^0$	$H_d/D_h = 0.25$	3.21
2.	$\varphi = 4\%$, $n_p = 30$, $H_d/D_h = 0.25, P_d/H_d = 2.5$ and $\alpha_a = 60^0$	$H_d/d_p = 1.0$	3.21
3.	$\varphi = 4\%$, $n_p = 30, H_d/D_h = 0.25$, $H_d/d_p = 1.0$ and $\alpha_a = 60^0$	$P_d/H_d = 2.5$	3.21
4.	$\varphi = 4\%, n_p = 30$, $H_d/D_h = 0.25$, $H_d/d_p = 1.0$ and $P_d/H_d = 2.5$	$\alpha_a = 60^0$	3.21

10. DEVELOPMENT OF CORRELATIONS FOR Nu_{rs} AND f_{rs}

The experimental data of the investigation reveals that the Nu_{rs} and f_{rs} are strong functions of the system and the operating parameters. The relationship of Nu_{rs} and f_{rs} with the governing parameters can be functionally written as

$$Nu_{rs} = f_1(Re, \varphi, n_p, H_d/D_h, H_d/d_p, P_d/H_d, \alpha_a/60) \quad (36)$$

$$f_{rs} = f_2(Re, \varphi, n_p, H_d/D_h, H_d/d_p, P_d/H_d, \alpha_a/60) \quad (37)$$

The data collected have been utilized to develop statistical correlations for the Nusselt number and friction factor using regression analysis. The development of correlation starts with plotting $ln(Nu_{rs})$ and $ln(Re)$ for all the data points. Functional relationship between $Nu_{rs}$and Re is obtained by regression analysis as shown in Fig. 14.

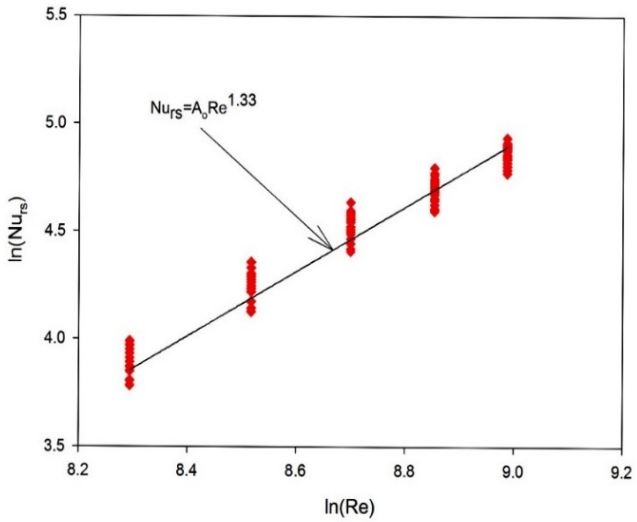

Fig. 14 Plot of ln(Nu_{rs}) as function of ln(Re) for all the experimental data.

Global Digital Central
ISSN: 2151-8629

By curve fitting a straight line is generated through these points and is given by

$$Nu_{rs} = A_0 Re^{1.33} \quad (38)$$

where A_0 is functionally depending on other system parameter i.e.φ. The value of $(Nu_{rs}/Re^{1.33} = A_0)$ is plotted on the log–log scale, as a function of φas shown in Fig. 15.

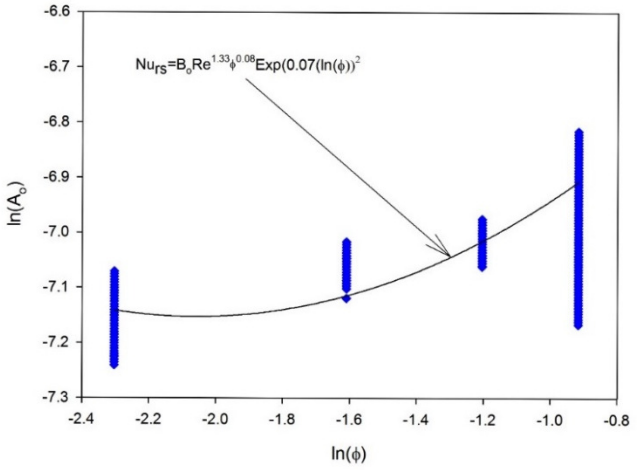

Fig. 15 Plot of $ln(A_0)$ as function of $ln(\varphi)$.

A second-order polynomial equation using regression analysis is generated and is given by

$$\ln[Nu_{rs}/Re^{1.33}] = lnB_0 + A_{11}\ln(\varphi) + A_{12}(\ln(\varphi))^2 \quad (39)$$

The above equation can be rearranged as

$$[Nu_{rs}/Re^{1.33}] = B_0(\varphi)^{0.08}\exp[0.07(ln(\varphi))^2] \quad (40)$$

where B_0 is the function of system parametern_p. A log–log scale plot between B_0, and n_p is shown in Fig. 16. A curve fitting by second-order polynomial is given by:

$$ln\left[\frac{Nu_{rs}}{Re^{1.33}\varphi^{0.08}Exp[0.07(\ln(\varphi))^2]}\right] = C_O n_p^{1.25} Exp\left(-0.21\left(\ln\left(n_p\right)\right)^2\right) \quad (41)$$

where C_0 is the function of $H_d/D_h$and is platted on a log–log scale.

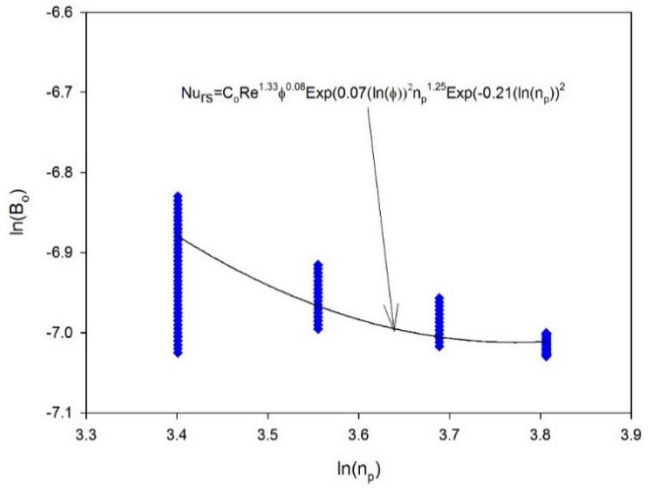

Fig. 16 Plot of $ln(B_o)$ as function of $ln(n_p)$.

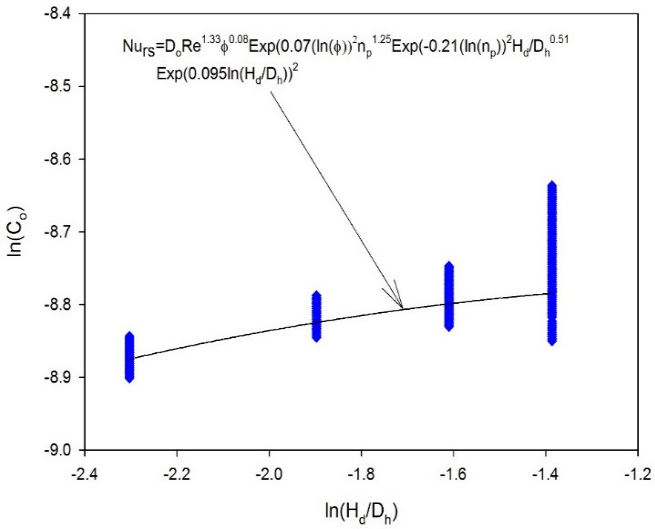

Fig. 17 Plot of $ln(C_0)$ as function of $ln(H_d/D_h)$.

Fig. 17 shows a regression analysis second- order polynomial curve fitting and the equation is given by

$$ln\left[\frac{Nu_{rs}}{Re^{1.33}\varphi^{0.08}Exp[0.07(\ln(\varphi))^2]n_p^{1.25}Exp(-0.21\left(\ln\left(n_p\right)\right)^2)}\right] = D_0\left(\frac{H_d}{D_h}\right)^{0.51} Exp(0.095(ln(H_d/D_h)))^2 \quad (42)$$

where D_0 is the function of $H_d/d_p$and is platted on a log–log scale.

Fig. 18 shows a regression analysis second- order polynomial curve fitting and the equation is given by

$$ln\left[\frac{Nu_{rs}}{Re^{1.33}\varphi^{0.08}Exp[0.07(\ln(\varphi))^2]n_p^{1.25}Exp\left(-0.21\left(\ln\left(n_p\right)\right)^2\right)}{(H_d/D_h)^{0.51}Exp(0.095(\ln(H_d/D_h)))^2}\right] = D_0\left(\frac{H_d}{D_h}\right)^{-0.07} Exp(-0.19(ln(H_d/D_h)))^2 \quad (43)$$

where $E_0$is the function of P_d/H_d and is platted on a log–log scale.

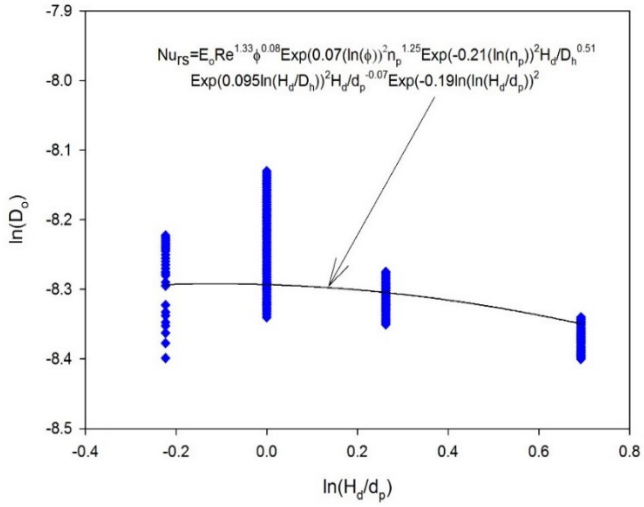

Fig. 18 Plot of $ln(D_0)$ as function of $ln(H_d/d_p)$.

Global Digital Central
ISSN: 2151-8629

Fig. 19 shows a regression analysis second- order polynomial curve fitting and the equation is given by

$$ln\left[\frac{Nu_{rs}}{Re^{1.33}\varphi^{0.08}Exp[0.07(\ln(\varphi))^2]n_p^{1.25}Exp\left(-0.21\left(\ln\left(n_p\right)\right)^2\right)}\right.$$
$$\left.\times\left(H_d/d_p\right)^{-0.07}Exp(=0.19(\ln\left(H_d/d_p\right)))^2\right]$$
$$=E_0\left(\frac{P_d}{H_d}\right)^{2.35}Exp(-1.35(ln(P_d/H_d)))^2 \quad (44)$$

where F_0 is the function of α_a and is platted on a log–log scale.

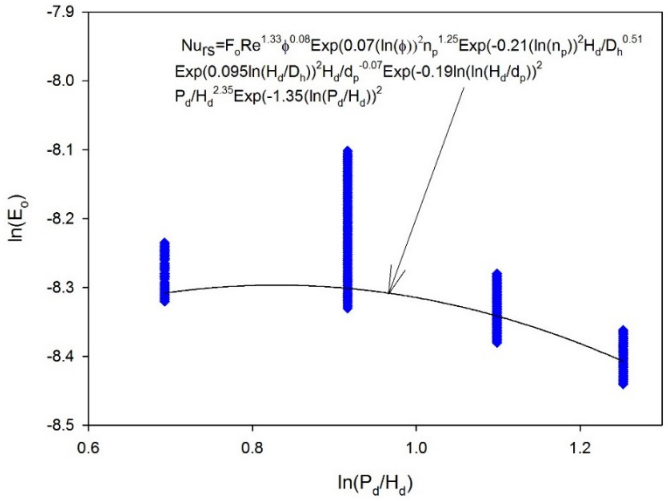

Fig. 19 Plot of $\ln(E_0)$ as function of $ln(P_d/H_d)$.

Fig. 20 shows a regression analysis second- order polynomial curve fitting and the equation is given by

$$ln\left[\frac{Nu_{rs}}{Re^{1.33}\varphi^{0.08}Exp[0.07(\ln(\varphi))^2]n_p^{1.25}Exp\left(-0.21\left(\ln\left(n_p\right)\right)^2\right)}\right.$$
$$\times\left(H_d/d_p\right)^{-0.07}Exp($$
$$\left.=0.19(\ln\left(H_d/d_p\right)))^2(P_d/H_d)^{2.35}Exp(-1.35(ln(P_d/H_d)))^2\right]$$
$$=F_0\left(\frac{\alpha_a}{60}\right)^{-0.17}Exp(-0.54(ln(\alpha_a/60)))^2 \quad (45)$$

The regression analysis yields the values of coefficients as:
Ao = -7.1, Bo = -6.9, Co = -8.65, Do= -4.23, Eo= -8.23, Fo= -9.22 and Go= -0.54

The values of coefficients result in the correlation for the Nusselt number as

$$Nu_{rs}$$
$$=9.23$$
$$\times10^{-7}Re^{1.33}\varphi^{0.08}Exp[0.07(\ln(\varphi))^2]n_p{}^{1.25}Exp\left(-0.21\left(\ln\left(n_p\right)\right)^2\right)$$
$$(H_d/D_h)^{0.51}$$
$$Exp(0.095(\ln(H_d/D_h)))^2\left(H_d/d_p\right)^{-0.07}Exp(-0.19(\ln\left(H_d/d_p\right)))^2$$
$$(P_d/H_d)^{2.35}$$
$$Exp(-1.35(\ln((P_d/H_d)))^2(\alpha_a/60)^{-0.17}Exp(-0.54(ln(\alpha_a/60)))^2 \quad (46)$$

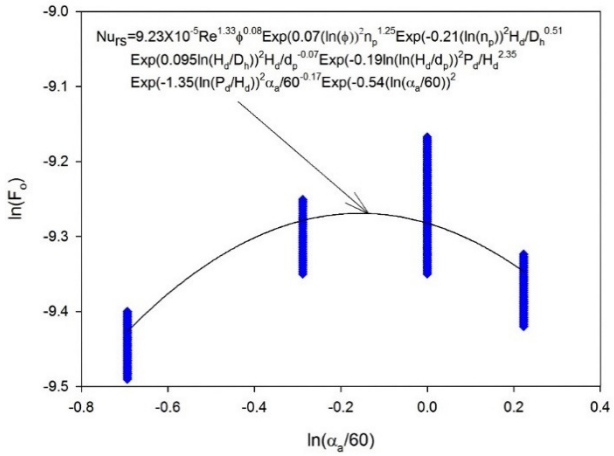

Fig. 20 Plot of $ln(Fo)$ as function of $\ln(\alpha_a/60)$.

A similarly regression analysis of experimental data of friction factor is carried out that yields to the correlation for the friction factor as given below and Fig.21 shows the regression analysis.

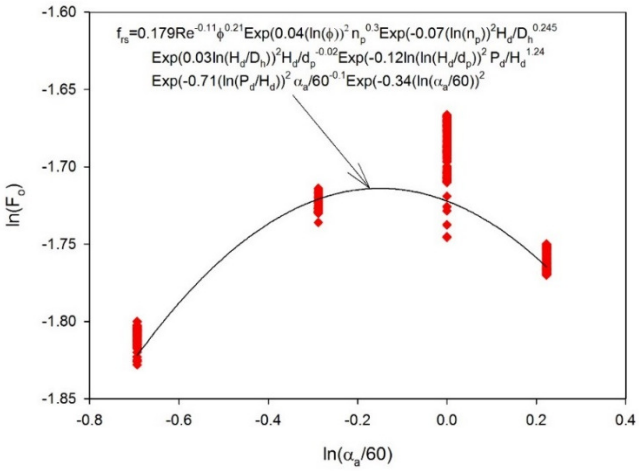

Fig. 21 Plot of $ln(Fo)$ as function of $\ln(\alpha_a/60)$.

$$f_{rs}$$
$$=0.17Re^{-0.11}\varphi^{0.21}Exp[0.04(\ln(\varphi))^2]n_p{}^{0.307}Exp\left(-0.07\left(\ln\left(n_p\right)\right)^2\right)$$
$$(H_d/D_h)^{0.24}$$
$$Exp(0.03(\ln(H_d/D_h)))^2\left(H_d/d_p\right)^{-0.02}$$
$$Exp(-0.12(\ln\left(H_d/d_p\right)))^2(P_d/H_d)^{1.24}$$
$$Exp(-71(\ln((P_d/H_d)))^2(\alpha_a/60)^{-0.109}Exp(-0.34(ln(\alpha_a/60)))^2 \quad (47)$$

The Nu_{rs} and f_{rs} values predicted from the correlations were compared with that of experimental values. Figs. 22 and 23 show the comparative graph of Nu_{rs} and f_{rs}, respectively. A deviation of experimental and predicted values of the Nu_{rs} and f_{rs} comes out to be $\pm$9.5% and $\pm$8.8%, respectively. The results show an acceptable agreement between the experimental and the predicted values of Nu_{rs} and f_{rs}.

Global Digital Central
ISSN: 2151-8629

11. CONCLUSIONS

This an experimental analysis of the Nu_{rs} and f_{rs} of $TiO_2 - H_2O$ based nanofluid flowing through a V-pattern protrusion ribbed square channel. The following conclusions can be drawn this analysis:

1. The effect of concentration, particle diameter, protrusion rib height, protrusion rib pitch, protrusion print diameter, flow attack angle and Reynolds number on thermal and hydrodynamics performance has been studied.
2. As compared to the smooth surface the V-pattern protrusion rib surface yields an increase of about 4.34 and 2.33 times in the Nu_{rs} and f_{rs}, respectively for the range of parameters investigated.
3. The highest improvement of thermal hydrodynamic performance is obtained at a range of φ = 4%, n_p = 30nm, H_d/D_h = 0.25, H_d/d_p = 1.0, P_d/H_d = 2.5 and α_a = 60^0 respectively. The maximum value of the thermal hydrodynamic performance was found to be 3.21 for the range of parameters examined.
4. Correlations have been developed for Nu_{rs} and f_{rs} as function of roughness and operating parameters. These correlations have been found predict the Nu_{rs} and f_{rs} values with deviation for $\pm 9.5\%$ and $\pm 8.8\%$ respectively.

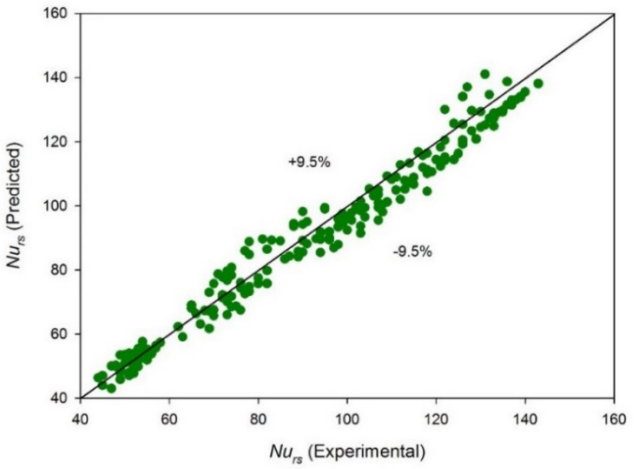

Fig. 22 Comparison of experimental and predicted values of Nusselt number.

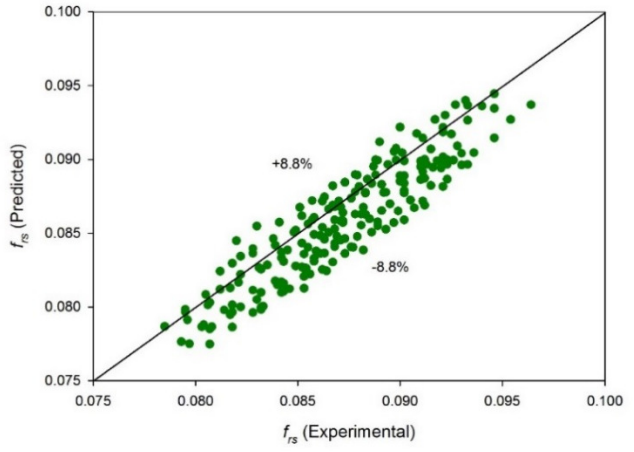

Fig. 23 Comparison of experimental and predicted values of friction factor.

NOMENCLATURE

A_p	Area of heated plate,m^2
d_H	Hydraulic diameter, m
f_{rs}	Friction factor, dimensionless ($f_{rs} = \frac{2\Delta P_0 D_h}{\rho_{nf} L_t {v_x}^2}$)
f_{av}	Average friction factor, dimensionless
h_c	Heat transfer coefficient, W/m^2K ($\frac{Q_u}{A_p \times \Delta T_f}$)
H_d/D_h	Ratio of V-pattern protrusion rib height
H_c	Height of channel, m
H_d/d_p	Ratio of V-pattern protrusion height to print diameter
k_{nf}	Thermal conductivity of nanofluid flow, W/mK
L_t	Length of test section, m
n_p	Particle diameter, nm
Nu_{rs}	Nusselt number of V-pattern protrusion rib
Nu_{av}	Average Nusselt number
P_d/H_d	Relative V-pattern protrusion rib pitch ratio
ΔP	Pressure drop across the test section, Pa
Q_u	Heat gain, W ($Q_u = m_a c_p \Delta T$)
Re	Reynolds number ($Re = \frac{\rho_{nf} \cdot v_x \cdot D_h}{\mu_{nf}}$)
T_{pt}	Weighted average plate temperature, K
T_{ft}	Average fluid temperature, K
W_c	Width of channel, m

Greek Letters

α_a	V-pattern protrusion rib flow attack angle, degree
ρ_{nf}	Density of nano fluid, kg/m^3
μ_{nf}	Dynamic viscosity of nano fluid, Ns/m^2
η_p	Thermal hydrodynamic performance, dimensionless
φ	Volume fraction, %

REFERENCES

Abdolbaqi, M.K., Azwadi, C.S.N., Mamat, R., 2014, "Heat transfer augmentation in the straight channel by using nanofluids", *Case Studies in Thermal Engineering* **3**:59–67.
http://dx.doi: 10.1016/j.csite.2014.04.001

Abed, A.M., Alghoul, M.A., Sopian, K., 2015, "Design characteristics of corrugated trapezoidal plate heat exchangers using nanofluids", *Chemical Engineering and Processing: Process Intensification* **87**:88–103.
http://dx.doi: 10.1016/j.cep.2014.11.005

Ahmed, H.E., Ahmed, M.I., Yusoff, M.Z., 2015a, "Heat transfer enhancement in a triangular duct using compound nanofluids and turbulators", *Applied Thermal Engineering* **91**:191–201.
http://dx.doi: 10.1016/j.applthermaleng.2015.07.061

Ahmed, H.E., Ahmed, M.I., Yusoff, M.Z., 2015b, "Experimental study of heat transfer augmentation in non-circular duct using combined nanofluids and vortex generator", *International Journal of Heat and Mass Transfer* **90**:1197–1206.
http://dx.doi: 10.1016/j.ijheatmasstransfer.2015.07.065

Ahmed, H.E., Mohammed, H.A., Yusoff, M.Z., 2012, "Heat transfer enhancement of laminar nanofluids flow in a triangular duct using vortex generator", *Superlattices and Microstructures* **52**:398–415.
http://dx.doi: 10.1016/j.spmi.2012.05.023

Ahmed, M.A., Yusoff, M.Z., Ng. K.C., Shuaib, N.H., 2014, "The effects of wavy-wall phase shift on thermal-hydraulic performance of Al2O3-

water nanofluid flow in sinusoidal-wavy channel", *Case Studies in Thermal Engineering* **4**:153–165.
http://dx.doi: 10.1016/j.csite.2014.09.005

Ahmed, M.A., Yusoff, M.Z., Shuaib, N.H., 2013, "Effects of geometrical parameters on the flow and heat transfer characteristics in trapezoidal-corrugated channel using nanofluid", *International Communications in Heat and Mass Transfer* **42**:69–74.
http://dx.doi: 10.1016/j.icheatmasstransfer.2012.12.012

Ahn, H.S., Kim. H., Jo, H.J., 2010, "Experimental study of critical heat flux enhancement during forced convective flow boiling of nanofluid on a short heated surface", *International Journal of Multiphase Flow* **36**:375–384.
http://dx.doi: 10.1016/j.ijmultiphaseflow.2010.01.004

Al-Shamani, A.N., Sopian, K., Mohammed, H.A., 2015, "Enhancement heat transfer characteristics in the channel with Trapezoidal rib-groove using nanofluids", *Case Studies in Thermal Engineering* **5**:48–58.
http://dx.doi: 10.1016/j.csite.2014.12.003

Andreozzi, A., Manca, O., Nardini S., Ricci D., 2016, "Forced convection enhancement in channels with transversal ribs and nanofluids", *Applied Thermal Engineering* **98**:1044–1053.
doi: 10.1016/j.applthermaleng.2015.12.140

Behnampour, A., Akbari, O.A., Safaei, M.R., 2017, "Analysis of heat transfer and nanofluid fluid flow in microchannels with trapezoidal, rectangular and triangular shaped ribs", *Physica E: Low-Dimensional Systems and Nanostructures* **91**:15–31.
http://dx.doi: 10.1016/j.physe.2017.04.006

Chokphoemphun, S., Pimsarn, M., Thianpong, C., Promvonge, P., 2015, "Heat transfer augmentation in a circular tube with winglet vortex generators", *Chinese Journal of Chemical Engineering* **23**:605–614.
http://dx.doi: 10.1016/j.cjche.2014.04.002

Coleman, H.W., Steele, W.G., 2009, "Experimentation, Validation, and Uncertainty Analysis for Engineers", *Third Edition, John Wiley & Sons, Inc*., Hoboken.
doi:10.1002/9780470485682

Duangthongsuk, W., Wongwises, S., 2009, "Heat transfer enhancement and pressure drop characteristics of TiO2-water nanofluid in a double-tube counter flow heat exchanger", *International Journal of Heat and Mass Transfer* **52**:2059–2067.
http://dx.doi: 10.1016/j.ijheatmasstransfer.2008.10.023

Fang, X., Chen, Y., Zhang, H., 2016, "Heat transfer and critical heat flux of nanofluid boiling: A comprehensive review", *Renewable and Sustainable Energy Reviews* **62**:924–940.
doi:10.1016/j.rser.2016.05.047

Ganvir, R.B., Walke, P.V., Kriplani, V.M., 2017, "Heat transfer characteristics in nanofluid—A review", *Renewable and Sustainable Energy Reviews* **75**:451–460.
http://dx.doi: 10.1016/j.rser.2016.11.010

Haridas, D., Rajput, N.S., Srivastava, A., 2015, "Interferometric study of heat transfer characteristics of Al_2O_3 and SiO_2 based dilute nanofluids under simultaneously developing flow regime in compact channels", *International Journal of Heat and Mass Transfer* **88**:713–727.
http://dx.doi: 10.1016/j.ijheatmasstransfer.2015.05.027

Hassan, M.M., Teamah, M.A., El-Maghlany, W.M., 2016, "Numerical investigation for heat transfer enhancement using nanofluids over ribbed confined one-end closed flat-plate", *Alexandria Engineering Journal* 56:333-343.
http://dx.doi: 10.1016/j.aej.2017.03.051

Heyhat, M.M., Kowsary, F., Rashidi, A.M., 2012, "Experimental investigation of turbulent flow and convective heat transfer characteristics of alumina water nanofluids in fully developed flow regime", *International Communications in Heat and Mass Transfer* **39**:1272–1278.
http://dx.doi: 10.1016/j.icheatmasstransfer.2012.06.024

Ho, C.J., Chen, M.W., Li, Z.W., 2008, "Numerical simulation of natural convection of nanofluid in a square enclosure: Effects due to uncertainties of viscosity and thermal conductivity", *International Journal of Heat and Mass Transfer* **51**:4506–4516.
http://dx.doi: 10.1016/j.ijheatmasstransfer.2007.12.019

Khdher, A.B.M., Sidik, N.A.C., Mamat, R., Hamzah, W.A.W., 2015, "Experimental and numerical study of thermo-hydraulic performance of circumferentially ribbed tube with Al_2O_3 nanofluid", *International Communications in Heat and Mass Transfer* **69**:34–40.
http://dx.doi: 10.1016/j.icheatmasstransfer.2015.10.003

Khoshvaght-Aliabadi, M., Rahnama, P., Zanganeh, A., Akbari, M.H., 2016, "Experimental study on metallic water nanofluids flow inside rectangular duct equipped with circular pins (pin channel)", *Experimental Thermal and Fluid Science* **72**:18–30.
http://dx.doi: 10.1016/j.expthermflusci.2015.10.029

Kumar, S., Kothiyal, A.D., Bisht, M.S., Kumar, A., 2017a, "Turbulent heat transfer and nanofluid flow in a protruded ribbed square passage", *Results in Physics* **7**:3603–3618.
http://dx.doi: 10.1016/j.rinp.2017.09.023

Kumar, S., Kothiyal, A.D., Bisht, M.S., Kumar, A., 2017b, "Numerical analysis of thermal hydraulic performance ofAl2O3–H2Onanofluid flowing through a protrusion obstacles square mini channel", *Case Studies in Thermal Engineering* **9**:108-121.
http://dx.doi.org/10.1016/j.csite.2017.01.004

Lehtimaki, M,, Saamanen, a,, Taipale, a., 2002, "American Society of Heating, Refrigeration and Air Conditioning Engineers" (ASHRAE). Filtration 140.
http://dx.doi: 10.1615/atoz.a.amershrefaceng

Manca, O., Nardini, S., Ricci, D., 2012, "A numerical study of nanofluid forced convection in ribbed channels", *Applied Thermal Engineering* **37**:280–292.
http://dx.doi: 10.1016/j.applthermaleng.2011.11.030

Mohammed, H.A., Al-Shamani, A.N., Sheriff, J.M., 2012, "Thermal and hydraulic characteristics of turbulent nanofluids flow in a rib-groove channel", *International Communications in Heat and Mass Transfer* **39**:1584–1594.
http://dx.doi: 10.1016/j.icheatmasstransfer.2012.10.020

Nassan, T.H., Heris, S.Z., Noie, S.H., 2010, "A comparison of experimental heat transfer characteristics for Al_2O_3/water and CuO/water nanofluids in square cross-section duct", *International Communications in Heat and Mass Transfer* **37**:924–928.
http://dx.doi: 10.1016/j.icheatmasstransfer.2010.04.009

Navaei, A.S., Mohammed, H.A., Munisamy, K.M., 2015, "Heat transfer enhancement of turbulent nanofluid flow over various types of internally corrugated channels", *Powder Technology* **286**:332–341.

http://dx.doi: 10.1016/j.powtec.2015.06.009

Parsazadeh, M., Mohammed, H.A., Fathinia, F., 2013, "Influence of nanofluid on turbulent forced convective flow in a channel with detached rib-arrays", *International Communications in Heat and Mass Transfer* **46**:97–105.
http://dx.doi: 10.1016/j.icheatmasstransfer.2013.05.006

Pourdel, H., Afrouzi, H.H., Akbari, O.A., 2018, "Numerical investigation of turbulent flow and heat transfer in flat tube", *Journal of Thermal Analysis and Calorimetry* **8**:312-323.
http://dx.doi: 10.1007/s10973-018-7529-8

Sarkar, J., 2011, "A critical review on convective heat transfer correlations of nanofluids", *Renewable and Sustainable Energy Reviews* **15**:3271–3277.
doi: 10.1016/j.rser.2011.04.025

Tiwari, A.K., Ghosh, P., Sarkar, J., 2013, "Heat transfer and pressure drop characteristics of CeO2/water nanofluid in plate heat exchanger", *Applied Thermal Engineering* **57**:24–32.
https://doi.org/10.1016/j.applthermaleng.2013.03.047

Vajjha, R.S., Das, D.K., 2009, "Experimental determination of thermal conductivity of three nanofluids and development of new correlations", *International Journal of Heat and Mass Transfer* **52**:4675–4682.
http://dx.doi: 10.1016/j.ijheatmasstransfer.2009.06.027

Vanaki, S.M., Mohammed, H.A., 2015, "Numerical study of nanofluid forced convection flow in channels using different shaped transverse ribs", *International Communications in Heat and Mass Transfer* **67**:176–188. doi: 10.1016/j.icheatmasstransfer.2015.07.004

Vanaki, S.M., Mohammed, H.A., Abdollahi, A., Wahid, M.A., 2014, "Effect of nanoparticle shapes on the heat transfer enhancement in a wavy channel with different phase shifts", *Journal of Molecular Liquids* **196**:32–42.
http://dx.doi: 10.1016/j.molliq.2014.03.001

Vatani, A., Mohammed, H.A., 2013, "Turbulent nanofluid flow over periodic rib-grooved channels", *Engineering Applications of Computational Fluid Mechanics* **7**:369–381.
http://dx.doi: 10.1080/19942060.2013.11015478

Webb, R.L., Eckert, E.R.G., 1972, "Application of rough surfaces to heat exchanger design", *International Journal of Heat and Mass Transfer* **15**:1647–1658.
http://dx.doi: 10.1016/0017-9310(72)90095-6

Wen,D., Ding, Y., 2004, "Experimental investigation into convective heat transfer of nanofluids at the entrance region under laminar flow conditions", *International Journal of Heat and Mass Transfer* **47**:5181–5188.
http://dx.doi: 10.1016/j.ijheatmasstransfer.2004.07.012

Xu, H. Pop, I., 2014, "Fully developed mixed convection flow in a horizontal channel filled by a nanofluid containing both nanoparticles and gyrotactic microorganisms", *European Journal of Mechanics, B/Fluids* **46**:37–45.
https://doi.org/10.1016/j.euromechflu.2014.02.005

Zeinal, H.S,, Nasr, E.M., Etemad, S.G., 2007, "Experimental investigation of convective heat transfer of Al_2O_3/water nanofluid in circular tube", *International Journal of Heat and Fluid Flow* **28**:203–210. http://dx.doi: 10.1016/j.ijheatfluidflow.2006.05.001